



**HAL**  
open science

## **Integrating crystallisation into transmembrane chemical absorption: Process intensification for ammonia separation from anaerobic digestate**

C.J. Davey, M. Hermassi, E. Allard, M. Amine, N. Sweet, T. Schmieder Gaité,  
A. Mcleod, E.J. Mcadam

► **To cite this version:**

C.J. Davey, M. Hermassi, E. Allard, M. Amine, N. Sweet, et al.. Integrating crystallisation into transmembrane chemical absorption: Process intensification for ammonia separation from anaerobic digestate. *Journal of Membrane Science*, 2020, 611, pp.118236. 10.1016/j.memsci.2020.118236 . hal-02905252

**HAL Id: hal-02905252**

**<https://imt-mines-ales.hal.science/hal-02905252>**

Submitted on 26 Mar 2024

**HAL** is a multi-disciplinary open access archive for the deposit and dissemination of scientific research documents, whether they are published or not. The documents may come from teaching and research institutions in France or abroad, or from public or private research centers.

L'archive ouverte pluridisciplinaire **HAL**, est destinée au dépôt et à la diffusion de documents scientifiques de niveau recherche, publiés ou non, émanant des établissements d'enseignement et de recherche français ou étrangers, des laboratoires publics ou privés.

# Integrating crystallisation into transmembrane chemical absorption: Process intensification for ammonia separation from anaerobic digestate

C. J. Davey<sup>a</sup>, M. Hermassi<sup>a</sup>, E. Allard<sup>a,b</sup>, M. Amine<sup>a,b</sup>, N. Sweet<sup>c</sup>, T. Schmieder Gaité<sup>c</sup>, A. McLeod<sup>a</sup>,  
E. J. McAdam<sup>a,\*</sup>

<sup>a</sup>School of Water, Energy and Environment, Cranfield University, Bedfordshire, MK43 0AL, UK

<sup>b</sup>École des Mines d'Alès, 30319 ALÈS CEDEX, France

<sup>c</sup>Waste Resources Action Programme (WRAP), Banbury, OX16 5BH

## Highlights:

- Reactive crystallisation has been integrated into liquid-liquid membrane contactor.
- Reactive crystallisation within the lumen of a hydrophobic membrane contactor demonstrated for the first time.
- The use of an antisolvent is introduced to control solubility and maximise product yield.
- High quality crystalline ammonium sulphate can be produced as a saleable solid product.

## Abstract

In this study, reactive crystallisation is introduced into a liquid-liquid membrane contactor for the selective separation, purification and recovery of ammonia from concentrated waste. Whilst liquid-liquid membrane contactor technology has been previously demonstrated for ammonia absorption, further process intensification can be achieved by incorporating crystallisation into transmembrane chemisorption to recover the ammonia as crystalline ammonium sulphate. Reactive crystallisation occurred in the draw solution (sulphuric acid) which was supplied to the lumen-side of the polypropylene hollow-fibre. The ammonium sulphate concentration in the draw solution increased through ammonia mass transfer to supersaturation, at which time induction (the onset of nucleation) commenced. Ammonia mass transfer at draw concentrations above the solubility limit was not limited provided sufficient 'free' sulphate was available. This resulted in nucleation which occurred at a low level of supersaturation ( $C/C^*$ , 1.03) to produce small crystals of around 2.5  $\mu\text{m}$ , which indicated that nucleation was favoured. The nucleation rate was found to be proportional to the ammonia flux in the draw solution. As the solution became more saturated, crystal number increased but crystal growth was comparatively small; this is symptomatic of *reactive* crystallisation, where the rate of reaction exceeds the rate of mass transfer. Due to the large difference in the ratio between the lumen internal diameter and the mean crystal diameter ( $d_{\text{fibre}}/d_{\text{mean,CSD}}$ ,  $\sim 180$ ), no fibre clogging was observed despite facilitating crystallisation on the lumen-side of the membrane. Transmembrane chemisorption crystallisation presents a feasible process intensification for the selective separation of ammonia from environmental applications. For its integration into environmental applications, solutions to wetting and fouling remain due to associative interactions with the complex organic matrix that are practically achievable through engineering intervention. Subsequent transformation of ammonia into a crystalline phase of ammonium sulphate presents a new product which is of commercial interest.

**Keywords:** Membrane contactor; nitrogen; perstraction; hydrophobic; microporous; lumen-side crystallisation.

## 1. Introduction

Ammonia rich liquid wastes presently form environmentally harmful liquid emissions [1], and ammonia air emissions arising from the same facilities have also been linked to a rise in local mortality rate [2]. Consequently, regulations have been imposed to control disposal of treated ammonia rich digestate, with new regulations soon to be introduced to control the upstream fate of ammonia rich wastes, which will favour anaerobic digestion (AD) over landfill [3,4]. Due to these environmental drivers, the ammonia concentrations to be treated are increasing in concentration, which is exacerbated by the hydrolysis of high protein content biomass [4]. However, ammonia is toxic to methanogens, which inhibits biogas production and reduces energy production [5]. High ammonia concentrations in the final digestate is also a problem for final disposal as its spreading to land is restricted based on nitrogen content, which considerably increases tankering costs [6]. The economic incentive of providing a selective ammonia separation is therefore three-fold: (i) improved biogas production due to the removal of inhibitory ammonia, (ii) the reduction in ammoniacal nitrogen content of the digestate permitting an increase in local spreading; and (iii) developing a new revenue stream from the production of a new ammonia product.

Ammonia stripping is generally used for ammonia separation from slurries at full-scale [8-15]. This involves a two-stage process in which a high volume of air (exceeding  $1100 \text{ m}^3_{\text{air}} \text{ m}^{-3}_{\text{water}}$ ) is used within a packed column to liberate ammonia, with the arising ammonia enriched air subsequently passed into a second packed column for contacting with a sulphuric acid scrubbing solution that stabilises the ammonia as soluble ammonium sulphate:



Membrane contactor technology, incorporates a hydrophobic microporous membrane that supports a similar separation mechanism. However, since the hydrophobic membrane can provide non-dispersive contact between two fluids, the membrane can mediate transfer of ammonia directly between the ammonia rich digestate and the acid solution. This obviates the need for air stripping, therefore eliminating one treatment stage, and due to the higher interfacial area that can be incorporated into membrane contactors compared to packed columns (around 40 times greater interfacial area per unit

volume), considerable process intensification can be achieved [13]. The facilitated transport of ammonia between two fluids using membrane contactors, termed ‘perstraction’ [14] or ‘TransMembrane Chemisorption’ [15], has been studied by a number of authors. Although other acids have been demonstrated [16-18], almost all studies introduce the necessary chemical reaction to drive mass transfer through the introduction of a dilute sulphuric acid stream, of less than 5 % w/v [19-24]. This can achieve a maximum ammonium sulphate concentration of around 67 g (NH<sub>4</sub>)<sub>2</sub>SO<sub>4</sub> L<sup>-1</sup>, and is analogous to the commercial operation of conventional packed column ammonia strippers [25]. However, since the resultant ammonium sulphate concentration is significantly below the solubility limit of the salt (around 764 g kg<sup>-1</sup> @ 25 °C) [26], the end product comprises a considerable volume of dilute spent acid solution, rich in ammonium sulphate, which subsequently requires tankering and specialist disposal, incurring substantial cost.

Kieffer et al. [27,28] first introduced the concept of chemically reactive membrane crystallisation in which the controlled mixing of two solutes is facilitated by the membrane, to govern the rate at which the solubility limit of the salt is exceeded, in order to control nucleation. In their study, an over pressure was used to meter potassium sulphate solution [27,28] through the pores of a hydrophilic (polyethersulphone) hollow fibre ultrafiltration membrane into a barium chloride solution contained within the fibre lumen. The sparingly soluble barium sulphate salt (BaSO<sub>4</sub>, 0.000245 g 100 mL<sup>-1</sup>) was formed, which did not evidently initiate surface encrustation, and was successfully collected downstream provided the fibre lumen was of sufficient radii [27]. More recently, gas-liquid chemically-reactive membrane crystallisation has been demonstrated in which carbon dioxide diffuses through a hydrophobic (PTFE or polypropylene) membrane, into a reactive aqueous ammonia absorbent. Here, elevated membrane hydrophobicity lowers the free energy barrier for the formation of a critical nucleus, whilst a concentration gradient initiates at the porous wall through solute-solute counter diffusion, such that the controlled nucleation of ammonium bicarbonate was demonstrated [29].

In this study, we therefore propose to introduce chemically-reactive membrane crystallisation into the transmembrane chemisorption process for the separation and recovery of ammonia into crystalline ammonium sulphate within a single processing step. Whilst transmembrane chemisorption

is already notionally competitive versus conventional ammonia stripping methodologies due to the process intensification delivered, the capability of the membrane to facilitate the controlled nucleation and growth of crystalline ammonium sulphate, could significantly reduce the costs for ammonia saturated acid disposal, as disposal charges are generally based on ammonia load. The purification and consolidation of the ammonia into crystalline ammonium sulphate also changes the value proposition of the technology, since this can be used as a base chemical to numerous commercial applications [30]. Due to the high solubility of ammonium sulphate, elevated sulphuric acid concentrations are required to exceed the solubility limit and support the induction of heterogeneous nucleation at the membrane interface, which has not been previously studied in the literature. To date, most transmembrane chemisorption studies have deployed the feed within the fibre lumen [14]. However, in practice, for treatment of anaerobic digestate the feed should flow shell-side to simplify process operation in slurries [22]. Consequently, we propose to investigate lumen side crystallisation, analogous to Kieffer et al. [27,28] but using a hydrophobic membrane to provide the selective separation and transport of gas phase ammonia through the pore structure of the microporous wall to enable a counter diffusion chemical reaction between ammonia and sulphate to proceed adjacent to the membrane wall. This should favour the governance of heterogeneous nucleation at the fibre wall, where solid, liquid and gaseous phases intersect [29]. Particle size of the crystallised phase therefore becomes of critical importance, to limit fibre blocking but also because the market value of crystalline ammonium sulphate is reportedly size dependent [31]; the implementation of wide radius (I.D. = 1.2 mm) hydrophobic polypropylene microporous hollow fibres are therefore studied (Table 1). This will provide the first example of membrane crystallisation driven by chemical reaction, within a liquid-liquid membrane contactor configuration. As the product is highly soluble, the introduction of an antisolvent, in which ammonium sulphate is sparingly soluble, is also evaluated as a method to lower the solubility limit and increase product yield. Earlier studies have introduced the concept of antisolvent membrane crystallisation, in these an antisolvent is dosed into the crystallising solution through the pore structure of a membrane. The antisolvent dosing rate and therefore the rate of crystallisation is controlled by the pressure differential across the membrane between the shell and lumen [32,33]. Selection of a suitable antisolvent is crucial to any crystallisation process as it must be miscible with the main solvent used

whilst possessing sparing solubility of the solute to be precipitated. However, for use within a membrane contactor process it must also have additional suitable characteristics such as high surface tension, low volatility and high material compatibility so as not to influence the separation process. In the present research, the membrane is used to facilitate the ammonia-sulphuric acid reaction that occurs from the transport of ammonia across the membrane, which is expected to govern the rate of crystallisation, and we propose that an antisolvent can be introduced at a comparable rate to the inside of the lumen to increase yield whilst sustaining crystallisation within a metastable state. Specific objectives are therefore to: (i) investigate the influencing parameters for ammonia mass transfer, (ii) understand the influence on mass transfer resistance of increasing ammonium sulphate concentration on the draw side, (iii) demonstrate crystallisation of ammonium sulphate within the transmembrane chemisorption process for recovery of ammonia from an anaerobic rich analogue (at an environmentally relevant ammonia concentration), and; (iv) investigate the use of an antisolvent for additional control of supersaturation.

## **2. Materials and Methods**

### *2.1 Experimental set-up*

A single membrane fibre was potted within stainless steel connectors using a silicone sealant (E41, Elastosil, WACKER) and sealed in place with viton o-rings to ensure a liquid tight channel when placed in the custom module constructed of polyoxymethylene (POM) (Model Products, Bedford, UK). Polypropylene (PP) hydrophobic hollow fibre membranes (Accurel 300/1200) were used in all experiments (Table 1). The shell comprised a rectangular aperture (15 × 12 mm). Peristaltic pumps (Watson Marlow, UK) circulated the synthetic ammonia solution within the shell side and sulphuric acid solution within the lumen (Figure 1). Feed velocity was varied between 0.00095 and 0.04 m s<sup>-1</sup> and the stripping solution velocity varied between 0.05 and 0.59 m s<sup>-1</sup>. Dimethylsulfoxide (DMSO) was dosed into the draw solution at 0.063 mL min<sup>-1</sup> using a syringe pump (SP-50, Mettler Toledo, UK). All experiments were conducted at room temperature (23 °C ± 2).

## 2.2 *Materials and methods*

Ammonium Sulphate (98 %), Ammonium Chloride (98+ %), Sulfuric Acid (95 %), Dimethylsulfoxide (DMSO) (99+ %), Methanol (> 95 %), Acetone (> 95 %) and 2-propanol (> 95 %) were purchased from common laboratory suppliers (Fisher, UK; Sigma Aldrich, UK) and used as received. De-ionized water exhibited a resistivity of 10 M $\Omega$ .cm at 25 °C produced from a Purelab option ELGA pure water system. Feed ammonia concentration was fixed by addition of ammonium chloride to deionised water, and the pH adjusted using sodium hydroxide. The stripping solution consisted of sulfuric acid (50 g, unless otherwise stated) in deionised water (1 L total volume). Either ammonium chloride or ammonium sulphate were added to the stripping solution in varying quantities to mimic different degrees of ammonia recovery. Solubility measurements were conducted by addition of “excess” ammonium sulphate of known mass to 50 g of solution with a defined composition of water : antisolvent. Equilibrium between the two phases was achieved by stirring the slurries at room temperature (23 °C) for 18 h before filtering and drying of the recovered solid at 100 °C for 18 h. The solute mass balance was then completed after weighing the recovered dry solid to determine the dissolved solid [34].

Concentration of ammonia in the feed and stripping solution was monitored using a photometric method (Spectroquant<sup>®</sup> cell test 114559, Merck, UK) and pH measured with a pH meter (4330, Jenway, Stone, UK). Solution surface tension was measured with a Force Tensiometer (K6, Krüss, DE) using the Du Noüy ring method at room temperature (23 °C  $\pm$  2) and the average of three repeats reported. Membrane porosity was measured using a glass pycnometer (Fisher, UK), water and 2-propanol according to the method proposed by Smolders and Franken [35]. Membrane pore size was determined using the pressure step/stability method (Porolux 1000, Porometer, Be) with Porefil (16.3 dyn cm<sup>-1</sup>) as the wetting liquid. Contact angle was measured using the sessile drop method (OCA25, DataPhysics, DE) immediately after placing a 2  $\mu$ L drop of liquid on the membrane surface and is the average of 8 discrete measurements.

In-situ, real-time evaluation of crystallisation was undertaken using Focused Beam Reflectance Measurement (FBRM<sup>®</sup>) (G 400, Mettler-Toledo, UK), which provided chord length distributions. A

laser beam, rotated with high speed optics, set at  $2 \text{ m s}^{-1}$ , scanned a circular path in the flow, with particles measured via diffuse backscattered light. The focused beam crosses a particle on any straight line between the two edge points to provide a chord length measurement for that particle. The chord length distribution (CLD) was determined with iC FBRM<sup>®</sup> software using a window size of 10 samples smoothing and corresponding to subcategorization into 100 bins for a range of 1-500 microns with a logarithmic regulation spacing applied. The measurement volume per second of the FBRM ( $V$ ) was approximated as a rectangular cuboid [36]:

$$V = S \times W_l \times D_p \quad (2)$$

where  $S$  is scan speed of the laser ( $2 \text{ m s}^{-1}$ ),  $W_l$  the laser diameter ( $5.8 \times 10^{-6} \text{ m}$ ) and  $D_p$  the depth penetration of laser in solution ( $2 \times 10^{-4} \text{ m}$ ) which were assumed to be constant throughout the experiment allowing for estimation of the detectable number density  $N_m/V$ .

An immersed video microscope probe (Particle Vision and Measurement (PVM) (ParticleView (V19<sup>®</sup>), Mettler-Toledo, UK) was also used, which utilises reflected light illumination (8 pulsed laser diodes (4 front and 4 back) to collect  $2 \mu\text{m}$  resolution images with a field of view of  $1300 \mu\text{m} \times 890 \mu\text{m}$  ( $\pm 50 \mu\text{m}$ ). The back scattered light was detected by a charge-coupled device (CCD) element to construct grayscale images of  $1500 \times 1024$  pixels resolution.

### 3. Theory

Ammonia mass transport within a membrane contactor is composed of three resistances in series; feed side, membrane and permeate; the three steps comprising: (i) transfer of ammonia from the bulk solution across the boundary layer to the feed-side membrane surface; (ii) diffusion of ammonia gas through the membrane pores to the permeate side membrane-liquid interface and; (iii) reaction of ammonia with acid at the membrane stripping solution interface and diffusion of the salt into the bulk stripping solution. The overall mass transfer coefficient can therefore be described using a resistance in series model as [20]:

$$\frac{1}{K} = \frac{1}{K_f} + \frac{1}{K_m} + \frac{1}{K_p} \quad (3)$$

where  $K$  is the overall mass transfer coefficient,  $K_f$  is the feed side mass transfer coefficient,  $K_m$  is the membrane mass transfer coefficient, and  $K_p$  is the permeate side mass transfer coefficient. For membrane contactors operated with shell side flow parallel to the hollow fibres, Hasanoglu et al. [22] showed that the correlation of Prasad and Sirkar [38] (Equation 5) is valid for calculation of the feed side ammonia mass transfer coefficient ( $K_f$ ) for an outside-in hollow fibre configuration:

$$Sh = \frac{K_f d_e}{D_{a,w}} = \beta \left[ \frac{d_e(1 - \phi)}{L} \right] Re^{0.6} Sc^{0.33} \quad (4)$$

where  $\beta$  is a constant previously determined as 5.8 for a hydrophobic membrane used in a liquid-liquid extraction process [13],  $d_e$  is the equivalent diameter,  $\phi$  is the hollow fibre packing density,  $L$  is the module length,  $Re$  the Reynolds number,  $Sc$  the Schmidt number and  $D_{a,w}$  the diffusion coefficient of ammonia in water ( $1.5 \times 10^{-9}$  [39]). The Reynolds and Schmidt numbers can be calculated according to equations (5) and (6):

$$Re = \frac{d_e u \rho}{\mu} \quad (5)$$

$$Sc = \frac{\mu}{\rho D_{a,w}} \quad (6)$$

where  $u$  is the solution velocity,  $\rho$  is the solution density and  $\mu$  the viscosity of the solution. The values for solution density and viscosity were determined from data in [40]. The hollow fibre packing density can be calculated using:

$$\phi = N_F \left( \frac{d_{o.d.}}{D_{in,s}} \right) \quad (7)$$

where  $N_F$  is the number of hollow fibres,  $d_{o.d.}$  the outer diameter of the hollow fibre and  $D_{in,s}$  the internal diameter of the shell (the equivalent diameter  $d_e$  was used due to the rectangular nature of the shell used). The equivalent diameter of the shell can be calculated using:

$$d_e = \frac{1.3(ab)^{0.625}}{(a + b)^{0.25}} \quad (8)$$

where  $a$  and  $b$  are the length of either side of the rectangular duct. Estimation of the membrane mass transfer coefficient,  $K_m$ , was conducted using [20,41]:

$$K_m = \frac{D_M \varepsilon H}{\delta \tau} \quad (9)$$

where  $D_M$  is the diffusion coefficient of ammonia in the gas phase of the membrane pores,  $\varepsilon$  is the porosity of the membrane,  $H$  is Henry's constant relating the partitioning of ammonia concentration in the gas phase with the liquid phase ammonia concentration,  $\delta$  is the membrane wall thickness and  $\tau$  the tortuosity of the membrane which can be estimated from the porosity [42] according to the relationship:

$$\tau = \frac{(2 - \varepsilon)^2}{\varepsilon} \quad (10)$$

The gas diffusion through the membrane pores, defined by the diffusion coefficient  $K_m$ , can be described as either molecular diffusion, Knudsen diffusion or an intermediate between the two depending on the value of the Knudsen number:

$$Kn = \frac{\lambda}{d_p} \quad (11)$$

where  $\lambda$  is the molecular mean free path length (76 nm [22]) and  $d_p$  the mean pore diameter of the membrane. For this work  $Kn$  was 0.18 indicating that the effect of Knudsen diffusion is minimal ( $Kn < 1$ ). Therefore, the diffusion coefficient of ammonia in the gas phase ( $K_M$ ,  $\text{m}^2 \text{s}^{-1}$ ) through the membrane pores has been estimated using the relationship of Fuller, Schettler and Giddings [22,43]:

$$D_M = \frac{1 \times 10^{-7} T^{1.75} \left( \left( \frac{1}{M_A} \right) + \left( \frac{1}{M_g} \right) \right)^{\frac{1}{2}}}{P \left[ (\sum V_A)^{\frac{1}{3}} + (\sum V_g)^{\frac{1}{3}} \right]^2} \quad (12)$$

where  $T$  is the temperature (K),  $M_A$  is the molecular weight of ammonia (0.017  $\text{kg mol}^{-1}$ ),  $M_g$  the molecular weight of air (0.029  $\text{kg mol}^{-1}$ ),  $P$  the pressure (Pa),  $V_A$  ( $1.49 \times 10^{-5} \text{ m}^3$ ) and  $V_g$  ( $2.01 \times 10^{-5} \text{ m}^3$ ) the diffusion volumes for ammonia and air respectively [43]. The final resistance in series between the permeate side of the membrane and bulk stripping solution  $\left( \frac{1}{K_p} \right)$  is often ignored as the reaction of ammonia with sulfuric acid is fast and there is an excess of sulfuric acid in the stripping solution [20,22]. Therefore (2) reduces to:

$$\frac{1}{K} = \frac{1}{K_f} + \frac{1}{K_m} \quad (13)$$

Finally, the ammonia-ammonium liquid phase equilibrium complicates mass transfer as a shift in the equilibrium will result in a change in the feed side resistance due to either more or less free ammonia available to diffuse across the liquid-vapour interface:



For unbuffered solutions, such as this work, the feed solution pH will change dependent on ammonia removal, and as such the ammonia-ammonium equilibrium, affecting the feed side mass transfer coefficient. To account for this Zhu [20] proposed:

$$\frac{1}{K} = \left( \frac{1}{K_f} + \frac{1}{K_m} \right) \frac{1}{\alpha_{\text{NH}_3}^2} \quad (152)$$

where  $\alpha_{\text{NH}_3}$  is the fraction of free ammonia relative to the total concentration of ammonia and ammonium at the initial time. This work initially sets out to ascertain if the assumption of a negligible permeate side resistance  $\left( \frac{1}{K_p} \right)$  (Equations (13) and (15)) holds true when the composition of the stripping solution is modified to aid supersaturation and crystallisation of ammonium sulphate. Additional resistance to mass transfer imposed by varying stripping solution composition, or from crystal growth on the membrane surface would be detrimental to the overall process efficiency and would need to be understood in order to optimise mass transfer. To observe the effect of varying parameters on the overall mass transfer coefficient it was determined experimentally using:

$$\ln \left( \frac{c_0}{c_t} \right) = \frac{AKt}{V} \quad (16)$$

where  $c_0$  is the initial total ammonia concentration in the feed solution ( $\text{mol L}^{-1}$ ),  $c_t$  the total concentration of ammonia in the feed solution ( $\text{mol L}^{-1}$ ) at time  $t$  (s),  $A$  is the total membrane area ( $\text{m}^2$ ),  $K$  the mass transfer coefficient ( $\text{m s}^{-1}$ ) and  $V$  the volume of feed solution ( $\text{m}^3$ ) (derivation of (16) can be found in [44]).

Having determined crystal number at increasing levels of supersaturation using FBRM, the change in crystal number ( $\Delta N$ ) over a prescribed time period ( $\Delta t$ ) can be calculated and the average nucleation rate becomes [37]:

$$B(L, t) = \frac{\Delta N}{\Delta t} \quad (17)$$

The preference towards heterogeneous crystal nucleation on the membrane surface over that within the bulk solution was determined by comparison of the free energies of the two processes [29,45]:

$$\frac{\Delta G_{het}}{\Delta G_{hom}} = 0.25(2 + \cos \theta)(1 - \cos \theta)^2 \left[ 1 - \varepsilon \frac{(1 + \cos \theta)^2}{(1 - \cos \theta)^2} \right]^3 \quad (18)$$

where  $\Delta G_{het}$  and  $\Delta G_{hom}$  are the free energies of heterogeneous and homogeneous nucleation,  $\theta$  the contact angle between liquid and membrane surface, and  $\varepsilon$  the membrane porosity.

## 4. Results & Discussion

### 4.1 Influence of operating parameters on ammonia mass transfer

An increase in feed solution pH provided the greatest enhancement in ammonia mass transfer, where  $K$  increased from 0 to  $0.51 \times 10^{-5} \text{ m s}^{-1}$  when the pH was raised from 8 to 11 (Figure 2a). This can be explained by the shift in the ammonia-ammonium equilibrium toward gas phase ammonia. At this temperature, the relative proportion of free ammonia within the feed solution at pH 11 was around 97.5 % [26], which reduced feed side resistance due to the increased proportion of gas phase ammonia available for transfer from the bulk liquid to the gas phase of the membrane pores [14]. In practice, anaerobic digesters operate between 35 – 40 °C, which is above the feed temperature studied. The higher operating temperature will shift the acid dissociation constant in favour of ammonia, and will raise ammonia mass transfer at lower pH [5]. However, an increase, or decrease, in ammonia concentration from  $3.1 \text{ gNH}_4^+\text{-N L}^{-1}$  (and at equivalent pH and fluid velocity), did not impact on ammonia mass transfer (Figure 2b), which is comparable to previous observations [14]. The mass transfer coefficient developed in liquid-liquid perstraction is around two orders of magnitude below that described in gas-liquid mass transfer for analogous membrane contactor technology [46], due to the lower feed-side diffusion coefficient experienced in liquid rather than gas phase mass transfer. Slow diffusion coupled with the high solubility of ammonia in water [26], subsequently introduces resistance within the feed-side boundary layer such that mass transfer is dependent upon the availability of gas phase ammonia but is independent of the feed-side concentration, within the boundary conditions

studied; the feed-side concentration being comparable to those observed in full scale anaerobic matrices [5].

Increasing the feed solution velocity did reduce mass transfer resistance at the feed side of the hydrophobic membrane with  $K$  increasing from 0.43 to  $0.78 \times 10^{-5} \text{ m s}^{-1}$  when the feed solution velocity was raised from 0.00095 to  $0.041 \text{ m s}^{-1}$  (Figure 2c). This can be explained by the suppression of  $\text{NH}_4^+$  and subsequent replenishment of new reactant (free  $\text{NH}_3$ ) within the boundary layer [19,29]. However, when the counter reactant ( $\text{SO}_4^{2-}$ ) is in excess, and because of the high solubility of ammonia in solution, the relative contribution of the feed velocity to mass transfer should be negligible [19]. This was evidenced by the curtailing of the enhancement to mass transfer above a feed velocity of  $0.01 \text{ m s}^{-1}$ . A change in ammonia mass transfer was not observed, following an increase in draw solution velocity from 0.05 to  $0.59 \text{ m s}^{-1}$  (Figure 2d), which can be ascribed to the large excess of acid within the draw side boundary layer, combined with the fast kinetics of ammonia, introducing limited resistance to mass transfer [21]. Within the conditions studied, the model of Zhu et al. [20] (eq. 14) closely predicted ammonia mass transfer, confirming that mass transfer is primarily governed by the ionisation of ammonia in the feed (Figure 2). The relative independence of mass transfer from hydrodynamics is a unique case for this membrane contactor application, which would indicate that further optimisation would not yield significant change to the mass transfer coefficient; however, the substantive surface area per volume (around  $10,000 \text{ m}^2 \text{ m}^{-3}$ ) that can be achieved with contactors, enable over an order of magnitude process intensification versus packed column technology [46].

#### *4.2 Influence of draw-side ammonium sulphate concentration on resistance to mass transfer*

Whilst the feed comprises the primary resistance to mass transfer in this study as with others [14,16], an increase in draw-side resistance to mass transfer could occur during the accumulation of ammoniacal nitrogen in the draw-side toward crystallisation. Initial experiments were undertaken at sufficiently low acid concentration to avoid crystallisation and so determine the impact of a transition in concentration and reactivity in isolation (Figure 3). As the molar ratio of ammonium to sulphate increased within the draw solution from 0 to 0.75, the rate of mass transfer was not obviously impacted, which can be

explained by the presence of an excess of sulphuric acid (Figure 3a). Further increase in the  $(\text{NH}_4^+)_2 : \text{SO}_4^{2-}$  molar ratio to 1.0 and 1.5, decreased ammonia mass transfer significantly to  $4.2 \times 10^{-6}$  and  $2.3 \times 10^{-7} \text{ m s}^{-1}$  respectively. Resistance in series analysis confirmed the primary resistance to mass transfer residing in the draw-side above an  $(\text{NH}_4^+)_2 : \text{SO}_4^{2-}$  molar ratio of 1.0 (Table 2). This can be explained by the draw-side pH, which demonstrated insufficient free acid available to enable the instantaneous reaction of ammonia to ammonium within the gas-liquid interface initiated at the draw-side of the membrane [19]. Whilst the inclusion of an additional resistance to mass transfer ( $1/k_p$ ) differs from earlier studies [16,17], this third resistance will be encountered at full-scale, even if not seeking to crystallise, through recirculation of the draw solution to ensure the economic utilisation of the acid.

The impact of concentrating dissolved ammonium sulphate within the draw solution on mass transfer was studied by ensuring an excess of sulphuric acid (50 g) sufficient to sustain reactivity (Figure 3b). An increase in concentration was evaluated up to the solubility limit, of 42.5 wt% (at 20 °C) [26]. The progressive increase in  $(\text{NH}_4)_2\text{SO}_4$  from 0 to 37 wt% did not evidently diminish mass transfer, which suggests chemically reactive crystallisation can proceed without an obvious impact upon mass transfer. However, such an increase in ammonium sulphate concentration could change the physical characteristics of the draw solution, such as the solution surface tension which would increase the probability for membrane wetting [46]. Draw solutions containing concentrated ammonium sulphate comprised an equivalent surface tension to water at this temperature ( $72 (\pm 2) \text{ mN m}^{-1}$ ) demonstrating the accumulation of  $(\text{NH}_4)_2\text{SO}_4$  to have a negligible impact on the non-dispersive contact induced by the membrane up to the salts solubility limit (Figure 4). Although this example has evidenced the application of sulphuric acid, future comparison with the application of alternative acids such as phosphoric and nitric would aid in probing the absorption and crystallisation mechanism due to the role different solution reactivities and chemistries (e.g. viscosity) play, particularly at the elevated acid concentrations required for crystallisation.

### *4.3 Identification and application of an antisolvent for control of supersaturation*

The use of methanol (MeOH) and dimethylsulfoxide (DMSO) as antisolvents was investigated to determine their suitability for lowering the solubility limit of ammonium sulphate and increase total product yield (Figure 5a). Inclusion of either methanol or DMSO exhibited a similar reduction in ammonium sulphate solubility. A 10% inclusion of antisolvent reduced the solubility product by 19%, whereas a 90 % reduction in solubility was observed with 40 vol% antisolvent added. For reference, this is greater than possible with cooling crystallisation due to the low solubility-temperature dependency of ammonium sulphate, in which a  $\Delta T$  of 60°C corresponds to a reduction in solubility of only 20% [47]. The water liquid entry pressure for the polypropylene membrane is typical for a membrane contactor at 0.132 MPa (calculated from the Young-Laplace equation [48]). However, any lowering of solution surface tension through introduction of an antisolvent could induce breakthrough and subsequent mixing between the feed and draw solutions, due to the affinity of organic solvents for wetting low surface energy polymers such as polypropylene. The impact of DMSO on the relative change in solution surface tension was much lower compared to that of methanol [49], and would therefore be a more desirable antisolvent due to its lower propensity to invoke wetting of the membrane pores (Figure 5b). In addition, DMSO possesses a much lower vapour pressure (0.0556 kPa @ 20 °C) compared to methanol (13.02 kPa @ 20 °C) indicating a much lower propensity to diffuse across the liquid-vapour interface and contaminate the feed [26]. The impact of adding DMSO on mass transfer was investigated within the range 0 to 10% w/v, which is equivalent to reducing ammonium sulphate solubility from ~740 g kg<sup>-1</sup> to ~530 g kg<sup>-1</sup> (Figure 5a). An initial small decline in  $K_{ov}$  from 0.43 to 0.30×10<sup>-5</sup> m s<sup>-1</sup> was observed when DMSO was initially added to a concentration of 1 wt% (Figure 5c). However, the increase in DMSO concentration did not obviously diminish ammonia transfer across the membrane contactor. The maximum attainable ammonium sulphate yield can therefore be adjusted using either the reactant concentration to fix the maximum ammonium sulphate concentration that can be achieved in the bulk solution ( $C_{max,react}$ ), or to introduce an antisolvent to reduce the solubility limit ( $C^*$ ):

$$Yield = \frac{C_{max,react} - C^*}{C_{max,react}} \quad (3)$$

As an illustrative example, using 50% acid could enable up to 9.2M of ammonium sulphate to form ( $C_{max,react}$ ), which exceeds the solubility limit of 5.6M ( $C^*$ ), providing a theoretical recovery of 39% in crystalline form. Antisolvent addition of 10% DMSO reduces  $C^*$  to 4M, thus increasing crystalline recovery to 57%.

#### 4.4 Demonstration of crystallisation within the transmembrane chemisorption process

The simultaneous transfer of ammonia and subsequent crystallisation of ammonium sulphate was investigated to elucidate the reaction conditions necessary for heterogeneous nucleation and crystallisation within the transmembrane chemisorption process. In the first phase, for reactive crystallisation to proceed, the membrane contactor was started with a draw solution consisting of an undersaturated ammonium sulphate solution ( $C/C^* = 0.99$ ) comprising an excess of sulphuric acid (Figure 6). Ammonia transferred across the membrane from feed to draw solutions raising the concentration of ammonium sulphate to a supersaturation ratio ( $C/C^*$ ) of 1.03 within 8.5 h at which time crystallisation was first determined by FBRM, the distribution for which comprised a primary peak centred at a chord length of 2.5  $\mu\text{m}$  (Figure 7a). Whilst crystal number increased with supersaturation level, chord length was predominantly below 10  $\mu\text{m}$  (Figure 7a) which suggests favouring primary heterogeneous nucleation, over crystal growth [50]. This is supported by estimation of the free energy change enabled by the polypropylene membrane employed in this study ( $\theta_{membrane-draw}$ , 128°;  $\epsilon$ , 0.73) which confirms the thermodynamic favourability for supported heterogeneous nucleation (Equation (18)). McLeod et al. [29] also demonstrated the potential significance of the reduction in surface free energy of their hydrophobic PTFE membrane to promoting crystal nucleation at low supersaturation ratios during reactive crystallisation [29]. Induction at a low level of supersaturation can be projected for ammonium sulphate due to its low interfacial energy (58.2  $\text{mJ m}^{-2}$ ; [51]). However, dominant nucleation in this case can be accounted for by the ratio of reactivity to mass transfer (analogous to the *Hatta* number), which in this study is characterised by fast kinetics and also mass transfer such that the reactant is quickly consumed within the reaction zone, sufficient to limit the slow

process of crystal growth [45]. In this study, the initial nucleation rate was comparable to those identified in membrane distillation crystallisation [52] but declined in proportion with ammonia flux (Figure 7b). This can be explained by the progressive consumption of available acid, as evidenced by the increasing transient in draw-side pH (Figure 6a), which usefully demonstrates that reactive crystallisation is directly dependent upon ammonia mass transfer across the membrane contactor.

Since the kinetics for ammonia mass transfer are zero order with respect to acid concentration [53], nucleation rate could be sustained at the same rate, through addition of excess reactant (acid). However, to improve the recovered yield, antisolvent addition is convenient, the crystallisation kinetics are then dependent upon the dose rate. Antisolvent dosing was instigated following cessation of the chemical reaction, at  $C/C^*$  1.06 (Figure 6) and re-initiation of ammonium sulphate crystallisation observed at a  $C/C^*$  of 1.1 (Figure 9). Broader distributions for chord length were identified with antisolvent addition than during reactive crystallisation, the peak of the distribution initially centred at 45  $\mu\text{m}$  for  $C/C^*$  1.1 and shifting to 90  $\mu\text{m}$  following higher rates of supersaturation (Figure 8a). Initial nucleation rate ( $112 \times 10^6 \text{ N m}^{-3} \text{ s}^{-1}$ ) was an order of magnitude higher than during reactive crystallisation (Figure 8b), which was confirmed with FBRM by the higher number count observed for each distribution (Figure 8a). Previous examples of antisolvent membrane crystallisation have utilised the membrane as a means of controlling the rate of addition of antisolvent / crystallisation solution [33]. The crystal growth observed in this study following dosing of antisolvent post reactive crystallisation can be attributed to secondary nucleation effects [54], rather than nucleation initiated at the membrane surface and is thermodynamically favoured when seed crystals are available [54]. The high nucleation rate is attributable to the antisolvent dose rate employed, which was at the minimum of the syringe pump ( $63 \mu\text{L min}^{-1}$ ). As demonstrated, DMSO exhibits promising qualities for use as an antisolvent within the transmembrane chemisorption crystallisation reactor, reducing ammonium sulphate solubility whilst providing negligible impact on surface tension and minimising the impact on ammonia mass transfer. Scale-up of the membrane for reactive crystallisation could enable the controlled addition of DMSO at an analogous rate to that of the reaction, such that both reactivity and crystal yield can be optimised.

Few studies have demonstrated crystallisation at the permeate side of the membrane, particularly within the lumen of a hollow fibre; osmotic or thermal concentrative driving forces are generally applied to crystallise within the feed-side. In this application, lumen-side crystallisation is critical, as the feed matrix (anaerobic digestate) is too complex for introduction into the lumen. The ratio of chord length (around 10 $\mu$ m) to lumen ID (1800  $\mu$ m) during reactive crystallisation was around  $d_p/f_{id}$  0.006 which would indicate minimal probability for clogging. Use of PVM enabled real time determination of the crystal phase during antisolvent crystallisation (Figure 9). The orthorhombic structure of ammonium sulphate could be visually determined from the images, and discrete crystals with chord lengths conforming to those identified with FBRM. Similarly, the ratio  $d_p/f_{id}$  of 0.06 would indicate negligible clogging, however, unlike during reactive crystallisation, crystal aggregates were produced (Figure 9a). Crystal aggregation can occur as a consequence of higher rates of nucleation [54], and can thus be controlled through lowering the rate of supersaturation. Nevertheless, during this study, retention of crystals within the fibre was not observed, which can be accounted for by the non-specific bond between membrane and crystal [45], and the limited physical restriction imposed by the wide diameter lumen employed. Although longer-term operation upon scale-up will inevitably result in some membrane wetting and scaling occurring from a build-up of precipitation in the fibre lumen, these results indicate that any required cleaning intervals would likely be infrequent and the non-specific bond between membrane and crystal indicates that standard chemical cleaning protocols would be a sufficient intervention. Ulbricht et al. [15] previously proposed crystallisation for transmembrane chemisorption but could not practically demonstrate this due to the temperature difference imposed ( $\Delta T$ , 20 to 30 °C) to promote ammonia mass transfer. However, the vapour pressure gradient established also induced water transport across the membrane, diluting the acid [15]. In this study, water transport was not observed, due to the small difference in water vapour pressure between solutions, and demonstrated feasibility to enable added value for industrial applications through recovery of a new resource.

## 5. Conclusions

This study provides the first demonstration of reactive crystallisation within a liquid-liquid membrane contactor for transmembrane chemisorption. The rate of nucleation in reactive crystallisation was found to be directly proportional to the ammonia flux across the membrane, which evidences the capability to manage the kinetic trajectory of crystallisation within membrane contactors. Whilst the rate of mass transfer ( $k_i$ ) is slow relative to gas-liquid membrane contactor applications, the overall mass transfer coefficient ( $K_{i,a}$ ) can be improved upon by increasing the specific surface area. Due to the relationship established between nucleation rate and ammonia mass transfer, nucleation should be predictable upon scale up. However, upon increasing surface area and fibre number, additional implications from water transport and fluid hydrodynamics will also need to be resolved, requiring precise design of module and process characteristics before full-scale implementation can be achieved. To initiate the level of supersaturation needed to induce nucleation, this study presented the first evidence on the impact of ammonium sulphate accumulation in the draw solution on the resistance to mass transfer and found that provided an excess of sulphuric acid is maintained, ammonia mass transfer remains unhindered and transmembrane reactive crystallisation can proceed. Due to the solubility product of ammonium sulphate, concentrated solution of acid is required and can be practically employed in membrane contactors due to material compatibility, whereas application of concentrated acids to standard packed columns would be more difficult. Herein, the crystallisation process differs from previous membrane crystallisation examples as the crystallisation is driven by chemical reaction rather than thermal gradient. Thermal gradients are difficult to apply to high solubility salts particularly ammonium sulphate which comprises of a 'flat' solubility-temperature dependency, thus in this study, the rate of reaction is governed by ammonia flux and the application of an antisolvent can be used to govern the thermodynamic solubility limit. Economic improvements can be made through solvent re-use of antisolvent, for example, where the higher freezing could permit for its facile separation. Whilst transmembrane chemisorption has been applied at scale for ammonia recovery from wastewater [15], application of the integrated crystallisation to this and to a wider range of ammonia rich liquid wastes such as digestate will require particular consideration of the impact the feed solution chemistries will

have on the process. However, the ability to crystallise within the membrane lumen and operate with feed on the shell side allows for the application of configurations suitable for managing such high organic and solid content feeds; for example, submerged modules are widely utilised in MBR applications for solid-liquid separation. The final purified and transformed ammonium sulphate crystalline phase could be valued comparatively to other forms of ammonium sulphate applied as fertiliser, which are commonly derived from waste ammonia sources, and could provide an additional revenue stream from the recovered ammonium sulphate (~ € 0.61 kgN<sup>-1</sup>).

## Acknowledgements

A. McLeod would like to thank the Waste and Resources Action Plan (WRAP) (Project #: OIN007). E. J. McAdam would like to thank ERC grant #714080. The findings and conclusions contained within are those of the authors and do not necessarily reflect positions or policies of the funders. Data underlying this paper can be accessed at: <https://doi.org/10.17862/cranfield.rd.12214400>

## References

- [1] D. Hogg, J. Barth, K. Schleiss, E. Favoino, *Dealing with Food Waste in the UK*, 2007.
- [2] F. Harvey, Dealing with ammonia is an urgent health problem – yet levels are still rising, *The Guardian* (2019). <https://www.theguardian.com/environment/2019/jun/13/ammonia-health-problem-rising-air-pollution> (Accessed 6th March 2020).
- [3] EU Landfill Directive (99/31/EC), n.d.
- [4] Scotland's Zero Waste Plan, Edinburgh, 2010. <http://www.gov.scot/Resource/0045/00458945.pdf>. (Accessed 6<sup>th</sup> March 2020)
- [5] O. Yenigün, B. Demirel, Ammonia inhibition in anaerobic digestion: A review, *Process Biochem.* 48 (2013) 901–911. <https://doi.org/10.1016/j.procbio.2013.04.012>.
- [6] The Nitrate Pollution Prevention Regulations 2008.
- [7] G. Saracco, G. Genon, High temperature ammonia stripping and recovery from process liquid wastes, *J. Hazard. Mater.* 37 (1994) 191–206. [https://doi.org/10.1016/0304-3894\(94\)85048-8](https://doi.org/10.1016/0304-3894(94)85048-8).

- [8] W. Tao, A.T. Ukwuani, Coupling thermal stripping and acid absorption for ammonia recovery from dairy manure: Ammonia volatilization kinetics and effects of temperature, pH and dissolved solids content, *Chem. Eng. J.* 280 (2015) 188–196. <https://doi.org/10.1016/j.cej.2015.05.119>.
- [9] K. Yetilmezsoy, Z. Sapci-Zengin, Recovery of ammonium nitrogen from the effluent of UASB treating poultry manure wastewater by MAP precipitation as a slow release fertilizer, *J. Hazard. Mater.* 166 (2009) 260–269. <https://doi.org/10.1016/j.jhazmat.2008.11.025>.
- [10] H. Huang, J. Liu, L. Ding, Recovery of phosphate and ammonia nitrogen from the anaerobic digestion supernatant of activated sludge by chemical precipitation, *J. Clean. Prod.* 102 (2015) 437–446. <https://doi.org/10.1016/j.jclepro.2015.04.117>.
- [11] A. Zarebska, D. Romero Nieto, K. V Christensen, B. Norddahl, Ammonia recovery from agricultural wastes by membrane distillation: Fouling characterization and mechanism, *Water Res.* 56 (2014) 1–10. <https://doi.org/10.1016/j.watres.2014.02.037>.
- [12] H.J. Lee, S.J. Oh, S.H. Moon, Recovery of ammonium sulfate from fermentation waste by electrodialysis, *Water Res.* 37 (2003) 1091–1099. [https://doi.org/10.1016/S0043-1354\(02\)00451-7](https://doi.org/10.1016/S0043-1354(02)00451-7).
- [13] A. Gabelman, S.-T. Hwang, Hollow fiber membrane contactors, *J. Memb. Sci.* 159 (1999) 61–106. [https://doi.org/10.1016/S0376-7388\(99\)00040-X](https://doi.org/10.1016/S0376-7388(99)00040-X).
- [14] M. Darestani, V. Haigh, S.J. Couperthwaite, G.J. Millar, L.D. Nghiem, Hollow fibre membrane contactors for ammonia recovery: Current status and future developments, *J. Environ. Chem. Eng.* 5 (2017) 1349–1359. <https://doi.org/10.1016/j.jece.2017.02.016>.
- [15] M. Ulbricht, J. Schneider, M. Stasiak, A. Sengupta, Ammonia Recovery from Industrial Wastewater by TransMembraneChemiSorption, *Chemie Ing. Tech.* 85 (2013) 1259–1262. <https://doi.org/10.1002/cite.201200237>.
- [16] E.E. Licon Bernal, C. Maya, C. Valderrama, J.L. Cortina, Valorization of ammonia concentrates from treated urban wastewater using liquid–liquid membrane contactors, *Chem. Eng. J.* 302 (2016) 641–649. <https://doi.org/10.1016/J.CEJ.2016.05.094>.
- [17] X. Vecino, M. Reig, B. Bhushan, O. Gibert, C. Valderrama, J.L. Cortina, Liquid fertilizer production by ammonia recovery from treated ammonia-rich regenerated streams using liquid-liquid membrane contactors, *Chem. Eng. J.* 360 (2019) 890–899. <https://doi.org/10.1016/J.CEJ.2018.12.004>.

- [18] M.M. Damtie, F. Volpin, M. Yao, L.D. Tijing, R.H. Hailemariam, T. Bao, K.-D. Park, H.K. Shon, J.-S. Choi, Ammonia Recovery from Human Urine as Liquid Fertilizers in Hollow Fiber Membrane Contactor: Effects of Permeate Chemistry, *Environ. Eng. Res.* (2020). <https://doi.org/10.4491/eer.2019.523>.
- [19] M.J. Semmens, D.M. Foster, E.L. Cussler, Ammonia removal from water using microporous hollow fibers, *J. Memb. Sci.* 51 (1990) 127–140. [https://doi.org/10.1016/S0376-7388\(00\)80897-2](https://doi.org/10.1016/S0376-7388(00)80897-2).
- [20] Z. Zhu, Z. Hao, Z. Shen, J. Chen, Modified modeling of the effect of pH and viscosity on the mass transfer in hydrophobic hollow fiber membrane contactors, *J. Memb. Sci.* 250 (2005) 269–276. <https://doi.org/10.1016/j.memsci.2004.10.031>.
- [21] X. Tan, S.P. Tan, W.K. Teo, K. Li, Polyvinylidene fluoride (PVDF) hollow fibre membranes for ammonia removal from water, *J. Memb. Sci.* 271 (2006) 59–68. <https://doi.org/10.1016/j.memsci.2005.06.057>.
- [22] A. Hasanoglu, J. Romero, B. Pérez, A. Plaza, Ammonia removal from wastewater streams through membrane contactors: Experimental and theoretical analysis of operation parameters and configuration, *Chem. Eng. J.* 160 (2010) 530–537. <https://doi.org/10.1016/j.cej.2010.03.064>.
- [23] F. Wäeger-Baumann, W. Fuchs, The Application of Membrane Contactors for the Removal of Ammonium from Anaerobic Digester Effluent, *Sep. Sci. Technol.* 47 (2012) 1436–1442. <https://doi.org/10.1080/01496395.2011.653468>.
- [24] B. Lauterböck, M. Ortner, R. Haider, W. Fuchs, Counteracting ammonia inhibition in anaerobic digestion by removal with a hollow fiber membrane contactor, *Water Res.* 46 (2012) 4861–4869. <https://doi.org/10.1016/j.watres.2012.05.022>.
- [25] J.W. Schroeder, A.C. Naso, USPAT 3,920, 419 Method of Removing Ammonia from Ammonia Containing Liquor, 1975. [https://doi.org/10.1016/0375-6505\(85\)90011-2](https://doi.org/10.1016/0375-6505(85)90011-2).
- [26] D.R. Lide, *CRC Handbook of Chemistry and Physics*, CRC Press, Boca Raton, FL, 2005. <https://doi.org/10.1021/ja906434c>.
- [27] R. Kieffer, D. Mangin, F. Puel, C. Charcosset, Precipitation of barium sulphate in a hollow fiber membrane contactor, Part I: Investigation of particulate fouling, *Chem. Eng. Sci.* 64 (2009) 1759–1767. <https://doi.org/10.1016/j.ces.2009.01.011>.

- [28] R. Kieffer, D. Mangin, F. Puel, C. Charcosset, Precipitation of barium sulphate in a hollow fiber membrane contactor: Part II The influence of process parameters, *Chem. Eng. Sci.* 64 (2009) 1885–1891. <https://doi.org/10.1016/j.ces.2009.01.013>.
- [29] A. McLeod, P. Buzatu, O. Autin, B. Jefferson, E. McAdam, Controlling shell-side crystal nucleation in a gas-liquid membrane contactor for simultaneous ammonium bicarbonate recovery and biogas upgrading, *J. Memb. Sci.* 473 (2015) 146–156. <https://doi.org/10.1016/j.memsci.2014.07.063>.
- [30] Ammonium Sulfate, (n.d.). <https://www.cropnutrition.com/ammonium-sulfate> (accessed December 5, 2019).
- [31] GEA, Ammonium Sulfate Fertilizer Industry, (2009).
- [32] D.M. Zarkadas, K.K. Sirkar, Antisolvent crystallization in porous hollow fiber devices, *Chem. Eng. Sci.* 61 (2006) 5030–5048. <https://doi.org/10.1016/j.ces.2006.03.036>.
- [33] E.D. Gianluca Di Profio, Carmen Stabile, Antonella Caridi, Efrem Curcio, Antisolvent Membrane Crystallization of Pharmaceutical Compounds, *J. Pharm. Sci.* 98 (2009) 4902. <http://onlinelibrary.wiley.com.ezproxy1.bath.ac.uk/wol1/doi/10.1002/jps.21785/full>.
- [34] S. Black, L. Dang, C. Liu, H. Wei, On the measurement of solubility, *Org. Process Res. Dev.* 17 (2013) 486–492. <https://doi.org/10.1021/op300336n>.
- [35] K. Smolders, A.C.M. Franken, Terminology for Membrane Distillation, *Desalination*. 72 (1989) 249–262. [https://doi.org/10.1016/0011-9164\(89\)80010-4](https://doi.org/10.1016/0011-9164(89)80010-4).
- [36] N.A. Mitchell, P.J. Frawley, C.T. Ó'Ciardhá, Nucleation kinetics of paracetamol–ethanol solutions from induction time experiments using Lasentec FBRM®, *J. Cryst. Growth*. 321 (2011) 91–99. <https://doi.org/10.1016/J.JCRYSGRO.2011.02.027>.
- [37] G. Chen, Y. Lu, X. Yang, R. Wang, A.G. Fane, Quantitative study on crystallization-induced scaling in high-concentration direct-contact membrane distillation, *Ind. Eng. Chem. Res.* 53 (2014) 15656–15666. <https://doi.org/10.1021/ie501610q>.
- [38] R. Prasad, K.K. Sirkar, Dispersion-free solvent extraction with microporous hollow-fiber modules, *AIChE J.* 34 (1988) 177–188.
- [39] Engineering ToolBox, (2001). <https://www.engineeringtoolbox.com> (accessed January 28, 2019).

- [40] M. Stefan-Kharicha, A. Kharicha, J. Mogeritsch, M. Wu, A. Ludwig, Review of Ammonium Chloride-Water Solution Properties, *J. Chem. Eng. Data.* 63 (2018) 3170–3183. <https://doi.org/10.1021/acs.jced.7b01062>.
- [41] C.F. Kenfield, R. Qin, M.J. Semmens, E.L. Cussler, Cyanide recovery across hollow fiber gas membranes, *Environ. Sci. Technol.* 22 (1988) 1151–1155. <https://doi.org/10.1021/es00175a003>.
- [42] L. Eykens, K. De Sitter, C. Dotremont, L. Pinoy, B. Van Der Bruggen, How To Optimize the Membrane Properties for Membrane Distillation: A Review, *Ind. Eng. Chem. Res.* 55 (2016) 9333–9343. <https://doi.org/10.1021/acs.iecr.6b02226>.
- [43] Robert H. Perry, D. Green, *Perry's Chemical Engineers' Handbook*, 50th ed., 1988.
- [44] E.L. Cussler, *Diffusion: Mass Transfer in Fluid Systems*, 2nd ed., Cambridge University Press, New York, 2000.
- [45] E. Curcio, E. Fontananova, G. Di Profio, E. Drioli, Influence of the structural properties of poly(vinylidene fluoride) membranes on the heterogeneous nucleation rate of protein crystals, *J. Phys. Chem. B.* 110 (2006) 12438–12445. <https://doi.org/10.1021/jp061531y>.
- [46] S. Heile, S. Rosenberger, A. Parker, B. Jefferson, E.J. McAdam, Establishing the suitability of symmetric ultrathin wall polydimethylsiloxane hollow-fibre membrane contactors for enhanced CO<sub>2</sub> separation during biogas upgrading, *J. Memb. Sci.* 452 (2014) 37–45. <https://doi.org/10.1016/J.MEMSCI.2013.10.007>.
- [47] Z. Zhu, Z. Zhu, P. Yin, Influence of Solubility of Ammonium Sulfate Caused by Decreasing pH or Adding Fe<sup>3+</sup> from (288.15 to 359.15) K, *J. Chem. Eng. Data.* 53 (2008) 565. <https://doi.org/10.1021/je7004243>.
- [48] T. Young, An essay on the cohesion of fluids. *Philos. T. R. Soc. Lond.*, 95, (1805) 65–87. <https://doi.org/10.1098/rspl.1800.0095>
- [49] W.J. Cheong, P.W. Carr, The Surface Tension of Mixtures of Methanol, Acetonitrile, Tetrahydrofuran, Isopropanol, Tertiary Butanol and Dimethyl-Sulfoxide with Water at 25°C, *J. Liq. Chromatogr.* 10 (1987) 561–581. <https://doi.org/10.1080/01483918708069009>.
- [50] J. W. Mullin, *Crystallization*, 4th Ed, Elsevier, 2001.

- [51] R. Mohan, O. Kaytancioglu, A.S. Myerson, Diffusion and cluster formation in supersaturated solutions of ammonium sulfate at 298 K, *J. Cryst. Growth.* 217 (2000) 393–403. [https://doi.org/10.1016/S0022-0248\(00\)00528-5](https://doi.org/10.1016/S0022-0248(00)00528-5).
- [52] X. Ji, E. Curcio, S. Al Obaidani, G. Di Profio, E. Fontananova, E. Drioli, Membrane distillation-crystallization of seawater reverse osmosis brines, *Sep. Purif. Technol.* 71 (2010) 76–82. <https://doi.org/10.1016/J.SEPPUR.2009.11.004>.
- [53] S.N. Ashrafizadeh, Z. Khorasani, Ammonia removal from aqueous solutions using hollow-fiber membrane contactors, *Chem. Eng. J.* 162 (2010) 242–249. <https://doi.org/10.1016/j.cej.2010.05.036>.
- [54] J.A. Dirksen, T.A. Ring, Fundamentals of crystallization: Kinetic effects on particle size distributions and morphology, *Chem. Eng. Sci.* 46 (1991) 2389–2427. [https://doi.org/10.1016/0009-2509\(91\)80035-W](https://doi.org/10.1016/0009-2509(91)80035-W).

## Figures

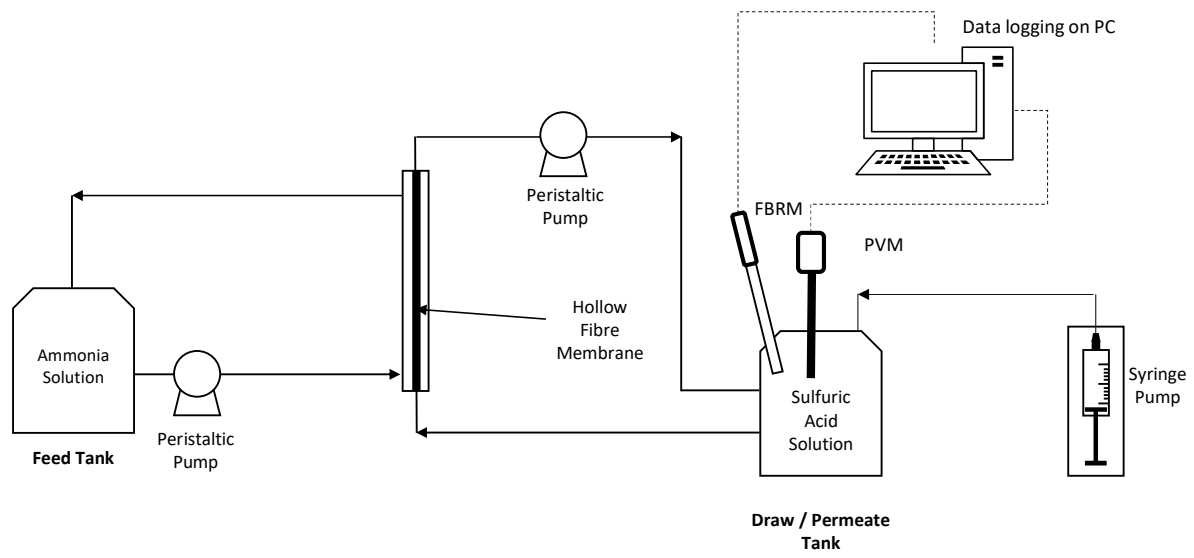


Figure 1. Schematic of the single hollow fibre experimental set-up used in all experiments.

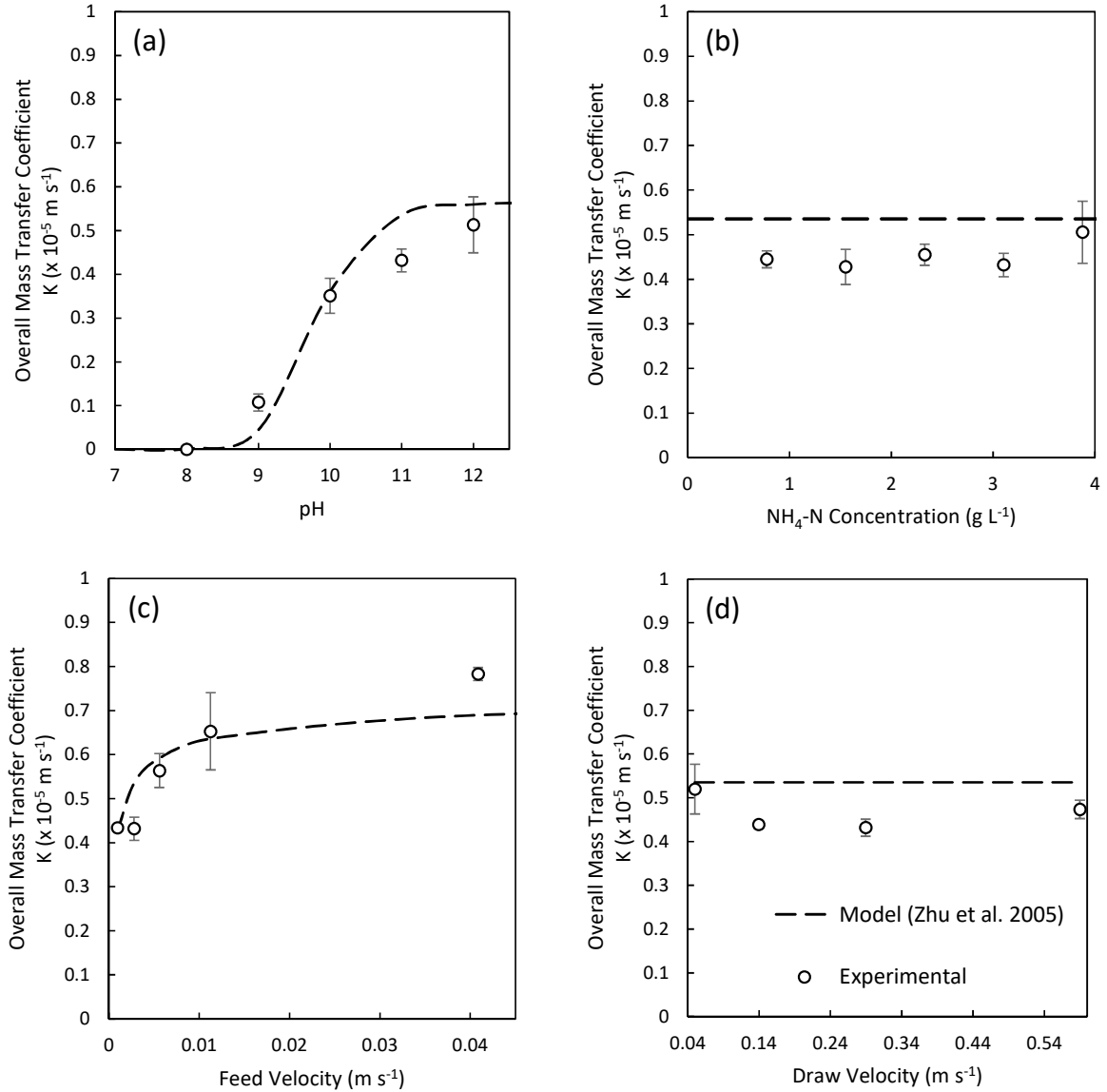


Figure 2. Effect of various process parameters on the overall mass transfer coefficient  $K$  (a) effect of feed pH, (b) effect of ammonium concentration in the feed, (c) effect of feed velocity and (d) effect of stripping solution velocity. (Standard Experimental Conditions:  $\text{pH}_{\text{Feed}} = 11$ ,  $[\text{NH}_4\text{-N}]_{\text{Feed}} = 3.1 \text{ g L}^{-1}$ ,  $[\text{H}_2\text{SO}_4]_{\text{Draw}} = 50 \text{ g L}^{-1}$ ,  $u_{\text{Feed}} = 0.0028 \text{ m s}^{-1}$ ,  $u_{\text{Draw}} = 0.29 \text{ m s}^{-1}$ ). Model predicted from Equation 14. Data points represent the average of three discrete experiments and error bars represent  $\pm \text{SD}$ .

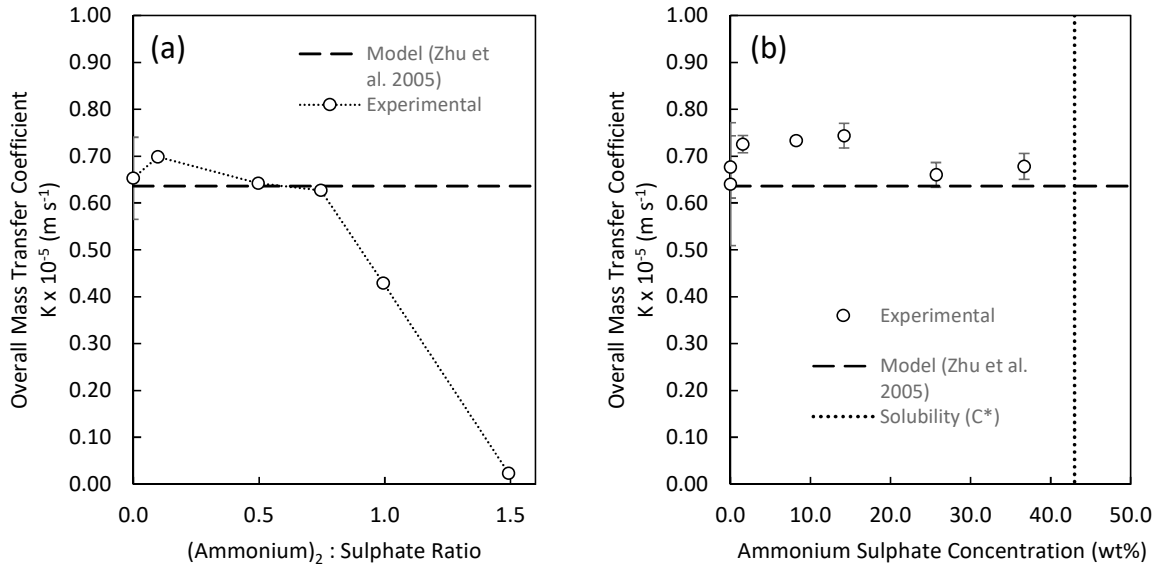


Figure 3. Influence of draw solution composition on the overall mass transfer coefficient: (a) increasing  $\text{NH}_4^+$  concentration in the draw solution ( $[\text{NH}_4\text{Cl}]_{\text{Draw}} = 0 - 87.1 \text{ g L}^{-1}$ ;  $[\text{H}_2\text{SO}_4]_{\text{Draw}} = 50 \text{ g L}^{-1}$ ;  $\text{pH}_{\text{Feed}} = 11$ ,  $[\text{NH}_4\text{-N}]_{\text{Feed}} = 3.1 \text{ g L}^{-1}$ ,  $u_{\text{Feed}} = 0.011 \text{ m s}^{-1}$ ,  $u_{\text{Draw}} = 0.29 \text{ m s}^{-1}$ ), (b) increasing  $(\text{NH}_4)_2\text{SO}_4$  concentration in the draw solution ( $[(\text{NH}_4)_2\text{SO}_4]_{\text{Draw}} = 0 - 450 \text{ g L}^{-1}$ ;  $[\text{H}_2\text{SO}_4]_{\text{Draw}} = 50 \text{ g L}^{-1}$ ;  $\text{pH}_{\text{Feed}} = 11$ ,  $[\text{NH}_4\text{-N}]_{\text{Feed}} = 3.1 \text{ g L}^{-1}$ ,  $u_{\text{Feed}} = 0.011 \text{ m s}^{-1}$ ,  $u_{\text{Draw}} = 0.29 \text{ m s}^{-1}$ ). Model predicted from Equation 14. Data points represent the average of three discrete experiments and error bars represent  $\pm \text{SD}$ .

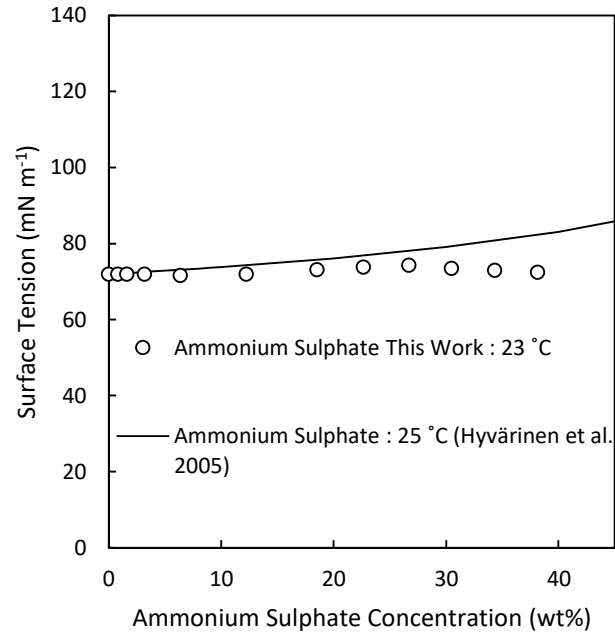


Figure 4. Effect of increasing ammonium sulphate concentration on solution surface tension. Data points represent the average of three discrete experiments, error bars represent  $\pm SD$  (obscured by data points).

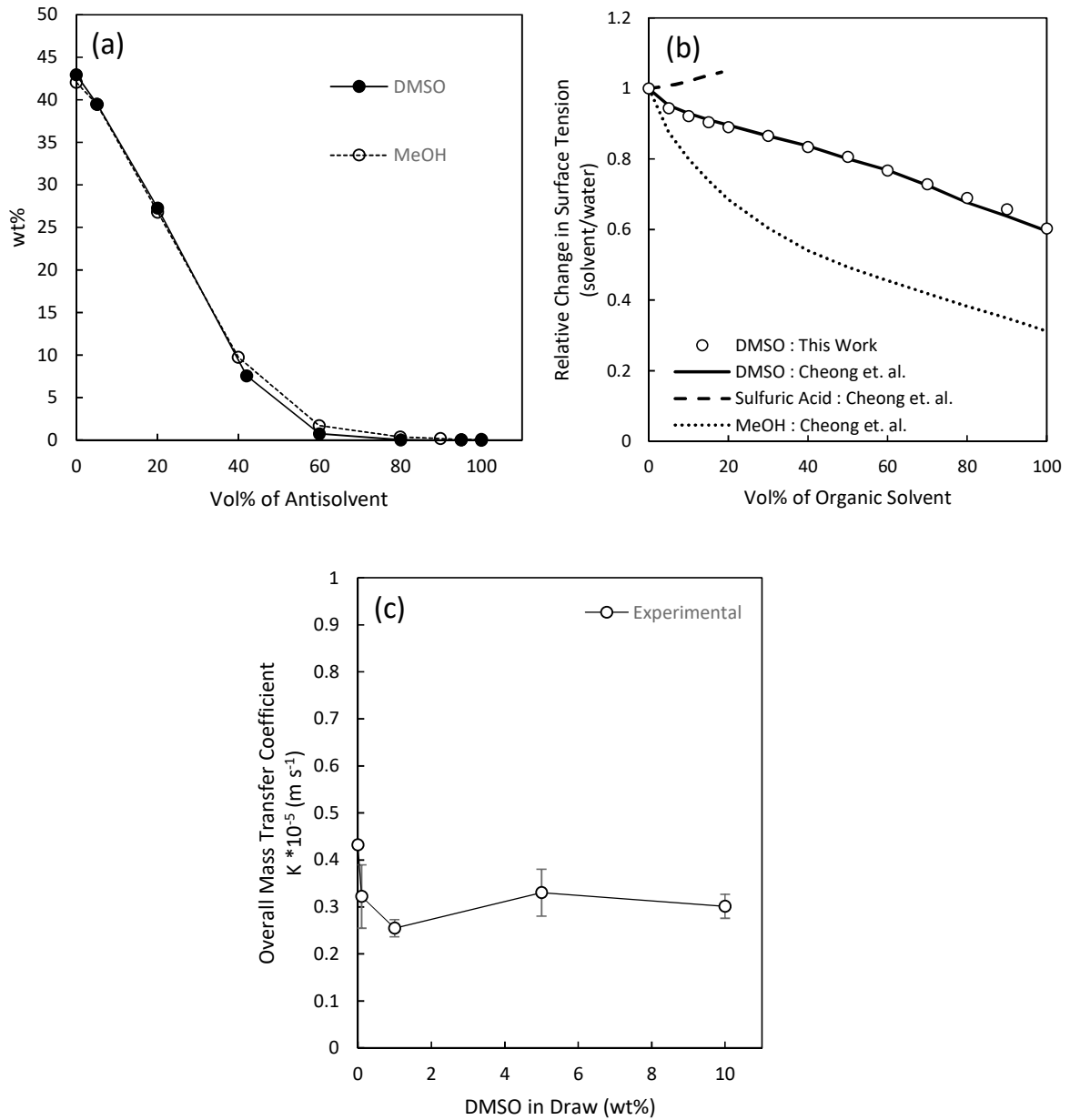


Figure 5. Anti-solvent characteristics: (a) Reduction in solubility; (b) relative change in solution surface tension; (c) effect on mass transfer coefficient ( $[DMSO]_{Draw} = 0 - 10 \text{ wt\%}$ ,  $[H_2SO_4]_{Draw} = 50 \text{ g L}^{-1}$ ,  $pH_{Feed} = 11$ ,  $[NH_4-N]_{Feed} = 3.1 \text{ g L}^{-1}$ ,  $u_{Feed} = 0.0028 \text{ m s}^{-1}$ ,  $u_{Draw} = 0.29 \text{ m s}^{-1}$ ). Data points represent the average of three discrete samples and error bars represent  $\pm \text{SD}$ .

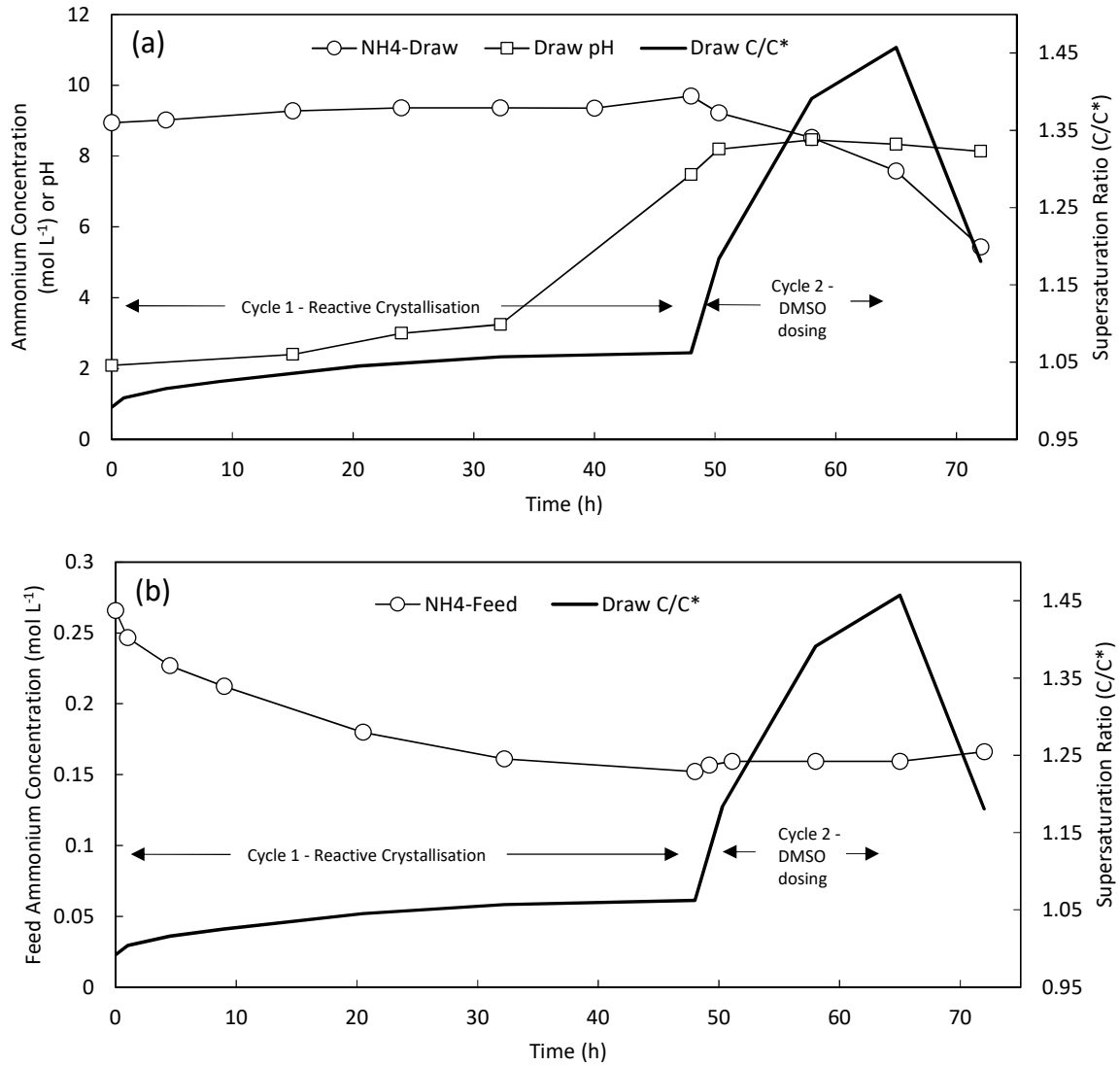


Figure 6. Ammonium concentration of the (a) draw and (b) feed solution over the course of the experiment and the relative supersaturation ratio of the draw solution ( $C/C^*$ ) (Standard Experimental Conditions:  $pH_{Feed} = 11$ ,  $[NH_4-N]_{Feed} = 3.1 \text{ g L}^{-1}$ ,  $[(NH_4)_2SO_4]_{Draw} = 748 \text{ g L}^{-1}$ ,  $[H_2SO_4]_{Draw} = 50 \text{ g L}^{-1}$ ,  $u_{Feed} = 0.011 \text{ m s}^{-1}$ ,  $u_{Draw} = 0.29 \text{ m s}^{-1}$ ).

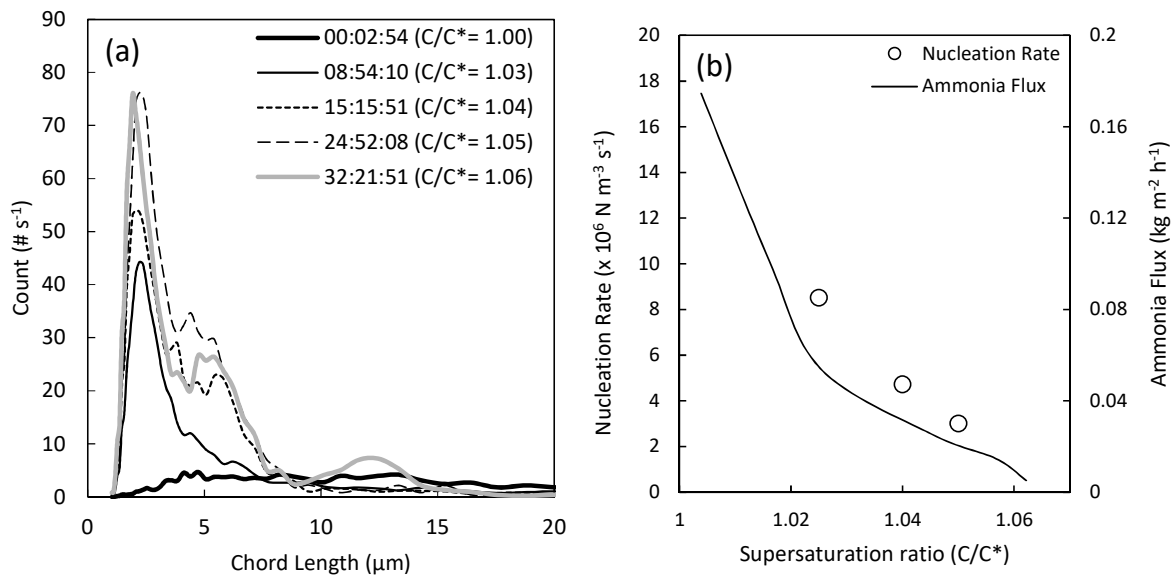


Figure 7. Analysis of FBRM data for the reactive crystallisation (a) crystal size distribution and (b) crystal nucleation rate compared to ammonia flux. Reduction in the crystal nucleation rate is proportional to ammonia mass transfer for the reactive crystallisation.

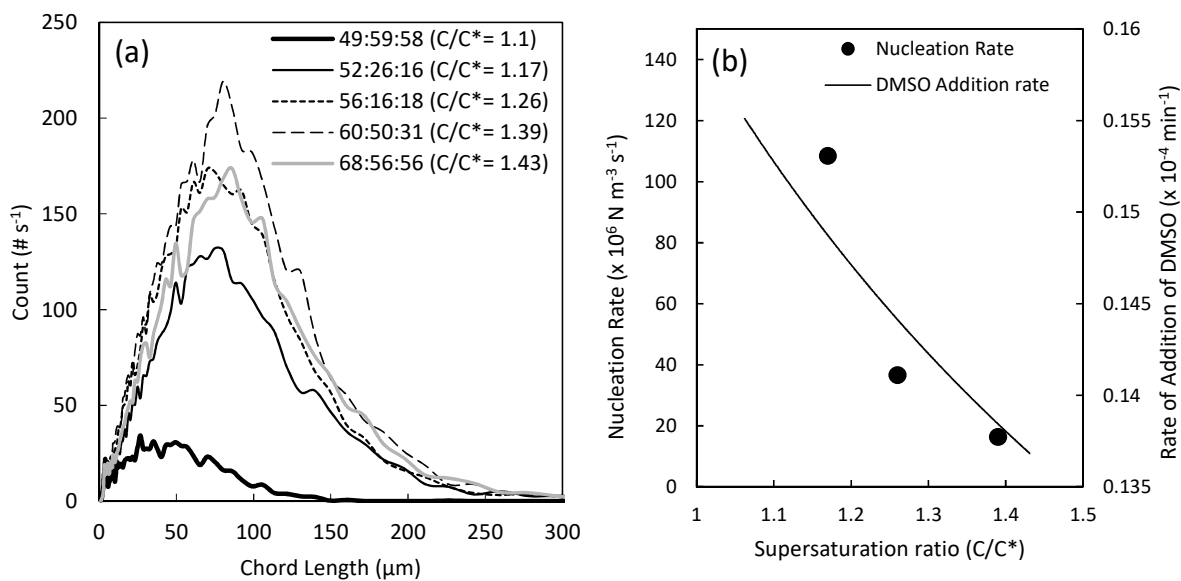
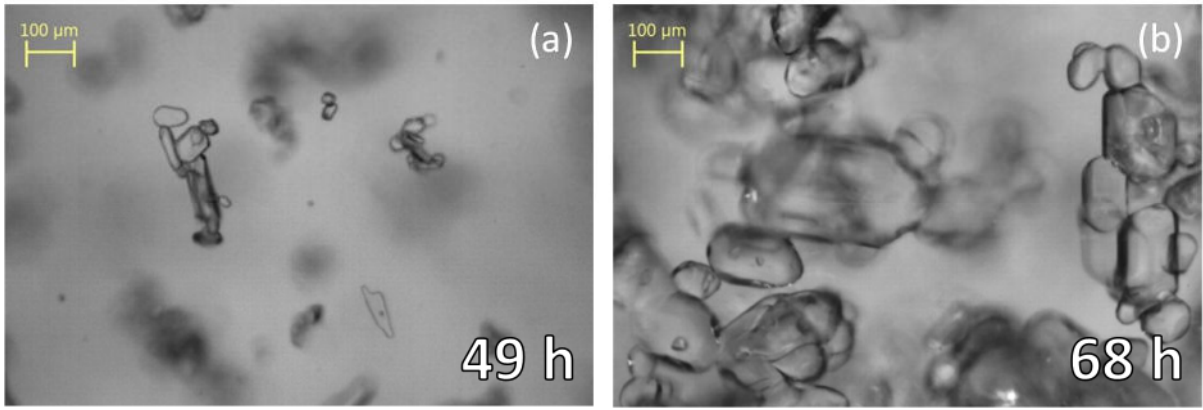


Figure 8. Analysis of FBRM data for anti-solvent crystallisation (a) crystal size distribution and (b) crystal nucleation rate compared to the relative rate of addition of DMSO. Reduction in the crystal nucleation rate is proportional to the dilution of the solution by the anti-solvent.



*Figure 9. In-situ PVM images of ammonium sulphate crystals formed in the draw solution whilst recycled through the membrane lumen during anti-solvent crystallisation. Images taken at (a) 49 h;  $C/C^* = 1.09$  and (d) 68 h;  $C/C^* = 1.35$ .*

## Tables

*Table 1. Membrane Material Details.*

Properties	Units	Dimensions/ attributes
Membrane Type		Accurel PP 300/1200
Material		Polypropylene
Fiber Dimensions	( $\mu\text{m}$ )	
Wall thickness		300
Internal diameter		1200
Outer diameter		1800
Measured Mean Pore Size ( $\mu\text{m}$ )		0.45
Surface Area	( $\text{m}^2$ )	$9.33 \times 10^{-4}$
Membrane Length	(m)	0.165
Measured Porosity	(%)	$73 \pm 2$
Measured water contact angle	( $^\circ$ )	131

*Table 2. Transition in resistance to mass transfer upon increasing draw-side concentration*

(NH <sub>4</sub> <sup>+</sup> ) <sub>2</sub> : SO <sub>4</sub> <sup>2-</sup> Ratio	1/K <sub>OV</sub>		1/k <sub>f</sub>		<sup>a,b</sup> 1/k <sub>m</sub>		1/k <sub>p</sub>	
	s m <sup>-1</sup>	(%)	s m <sup>-1</sup>	(%)	s m <sup>-1</sup>	(%)	s m <sup>-1</sup>	(%)
<0.75	153,846	100	28275	18.4	125,571	81.6	<sup>c</sup> n/a	n/a
1.0	238,095	100	28275	11.9	125,571	52.7	84,249	35.4
1.5	4,761,905	100	28275	0.59	125,571	2.6	4,608,059	96.8

<sup>a</sup>Based on Equation 8, where  $D_m$   $4 \times 10^{-6}$  m<sup>2</sup> s<sup>-1</sup>,  $\varepsilon$  0.73,  $H$   $1.8 \times 10^{-3}$ ,  $\tau$  2.25,  $\delta$   $300 \times 10^{-6}$  m. <sup>b</sup>1/k<sub>m</sub> of 97456 determined by Wilson plot. <sup>c</sup>Assumed negligible.